Journal of Nuclear Materials 402 (2010) 74–80

Contents lists available at ScienceDirect

Journal of Nuclear Materials

journal homepage: www.elsevier.com/locate/jnucmat

Physical properties of monolithic U8 wt.%–Mo

R.M. Hengstler [a,*], L. Beck [b], H. Breitkreutz [c], C. Jarousse [d], R. Jungwirth [c], W. Petry [c], W. Schmid [c], J. Schneider [e], N. Wieschalla [a]

[a] AREVA NP GmbH, Paul-Gossen-Str. 100, 91052 Erlangen, Germany
[b] Maier-Leibnitz-Laboratorium (MLL), Am Coulombwall 6, 85748 Garching, Germany
[c] Forschungsneutronenquelle Heinz Maier-Leibnitz (FRM II), Lichtenbergstr. 1, 85747 Garching, Germany
[d] AREVA-CERCA, A Subsidiary of AREVA NP, An AREVA and Siemens Company, Les Bérauds BP 114, 26104 Romans Cedex, France
[e] Ludwigs-Maximilians-Universität München, Department of Earth- and Environmental Sciences, Theresienstr. 41, 80333 München, Germany

ARTICLE INFO

Article history:
Received 27 May 2009
Accepted 24 April 2010

ABSTRACT

As a possible high density fuel for research reactors, monolithic U8 wt.%–Mo ("U8Mo") was examined with regard to its structural, thermal and electric properties. X-ray diffraction by the Bragg-Brentano method was used to reveal the tetragonal lattice structure of rolled U8Mo. The specific heat capacity of cast U8Mo was determined by differential scanning calorimetry, its thermal diffusivity was measured by the laser flash method and its mass density by Archimedes' principle. From these results, the thermal conductivity of U8Mo in the temperature range from 40 °C to 250 °C was calculated; in the measured temperature range, it is in good accordance with literature data for UMo with 8 and 9 wt.% Mo, is higher than for 10 wt.% Mo and lower than for 5 wt.% Mo. The electric conductivity of rolled and cast U8Mo was measured by a four-wire method and the electron based part of the thermal conductivity calculated by the Wiedemann-Frantz law. Rolled and cast U8Mo was irradiated at about 150 °C with 80 MeV ^{127}I ions to receive the same iodine ion density in the damage peak region as the fission product density in the fuel of a typical high flux reactor after the targeted nuclear burn-up. XRD analysis of irradiated U8Mo showed a change of the lattice parameters as well as the creation of UO_2 in the superficial sample regions; however, a phase change by irradiation was not observed. The determination of the electron based part of the thermal conductivity of the irradiated samples failed due to high measurement errors which are caused by the low thickness of the damage region in the ion irradiated samples.

1. Introduction

World wide efforts to reduce the usage of highly enriched uranium ("HEU") as fuel for research reactors make it mandatory to develop high density fuels [1]. The loss in enrichment has to be compensated by increasing the uranium density, such that the scientific quality of the respective neutron source is not altered. The alloy UMo with a content of 6–10 wt.% Mo is the most promising candidate for such a fuel. Depending whether UMo grains are dispersed in an Al matrix ("disperse fuel") or UMo is used in bulk form ("monolithic fuel"), densities of up to 8 gU/cm^3 [2] and 17 gU/cm^3 [3] are reachable. Engineering of new fuel assemblies requires, in addition to in-pile irradiations that have to prove the reliability of these new fuel materials, reliable values for UMo's thermal conductivity as a function of burn-up [3]. Because thermal conductivity strongly depends on the material's lattice structure, information about structural changes during in-pile irradiation is also needed.

The ability of UMo to contain the gaseous fission products is best in its high temperature γ-phase. To reliably quench the γ-phase to room temperature, a minimum of 6 wt.% Mo is needed, which sets the lower Mo content. Higher Mo concentrations stabilize the γ-phase further. The aim of the highest possible U density limits the maximum Mo concentration to 10 wt.%. Taking these considerations into account and knowing that in-pile irradiations using 7 wt.% Mo have failed, our work concentrates on UMo fuel with 8 wt.% Mo [2].

As the thermal properties of U8Mo and the behavior of its crystal lattice under irradiation are not available in the literature, these properties necessary for the new fuel qualification were examined and are described in this work. To avoid heavy activation and the following elaborate handling of the irradiated material, the fission products were simulated by ^{127}I ions of the typical fission product energy of 80 MeV; the irradiation has been carried out at the MLL tandem accelerator (Garching, Germany). There has been previous work proving that this method provides good accordance with irradiation damage by fission products in in-pile experiments [4–6].

Data on UMo lattice structures can be found for several Mo contents in the literature; however, U8Mo has not been studied,

* Corresponding author.
E-mail address: Rosmarie.Hengstler-Eger@areva.com (R.M. Hengstler).

0022-3115/$ - see front matter © 2010 Elsevier B.V. All rights reserved.
doi:10.1016/j.jnucmat.2010.04.024

neither unirradiated nor irradiated. Thus, X-ray diffraction on non-irradiated and iodine ion irradiated U8Mo samples were carried out at the Department of Earth- and Environmental Sciences of the Ludwigs-Maximilians-Universität (Munich, Germany).

Since the thermal properties of the fuel are necessary for the simulation and operation of the new fuel element's cooling system, the thermal conductivity of U8Mo was determined. That temperature dependent quantity can be calculated from the thermal diffusivity, the specific heat capacity and the mass density that were measured at AREVA NP GmbH (Erlangen, Germany).

With heat being conducted in metals by phonons and electrons, the electron based part of the thermal conductivity can be calculated from the electric conductivity of a metal by the Wiedemann-Frantz law. Thus, the electric conductivity of U8Mo was measured by a four-wire method.

The uranium in all samples was depleted (<0.25 wt.% ^{235}U) to simplify sample handling.

Last but not least, the present work is motivated by the search for a high density fuel which enables the reduction of enrichment in the compact core of the German neutron source Heinz Maier-Leibnitz (FRM II). Thus, irradiation doses were chosen to be comparable with the maximum fission product density in a FRM II fuel element at end of cycle conditions.

Table 1
List of UMo lattice structures.

Alloy; contents in atomic fraction	Structure	Lattice parameters (Å)	Density (g/cm^3)
U 1 (α) [10]	Orthorhombic Cmcm	a = 2.827 b = 5.845 c = 4.923	19.44
U 1 (γ) 774–1132 K [11]	Cubic Im-3m	a = 3.49	
Mo 0.10 U 0.90 [12]	Triclinic C-1	a = 2.866 b = 5.752 c = 4.940 γ = 92.28°	18.27
Mo 0.12 U 0.88 [13]	Tetragonal P4/nbm	a = 6.9244 c = 3.3998	18.01
Mo 0.14 U 0.86 (γ) [13]	Cubic Ia-3	a = 6.88	17.8
Mo 0.20 U 0.80 Measured	Tetragonal P4/nbm	a = 6.8563(4) c = 3.4524(2)	17.282
Mo 0.33 U 0.66 (MoU_2) [14]	Tetragonal I4/mmm	a = 3.427 c = 9.834	16.44
Mo 1 [15]	Cubic Im-3m	a = 3.14683	10.22

2. Sample preparation

For the different measurement setups used, small U8Mo samples of different dimensions were required; they were fabricated from cast and rolled U8Mo. The cast ingot was produced using an induction furnace. Via wire-electro discharge machining (WEDM) in a hot cell at AREVA NP GmbH (Erlangen, Germany), different samples were cut from this cast material: discs with diameter 8.39 mm and thicknesses from 0.5 mm to 2 mm were cut for laser flash and with thickness 4 mm for differential scanning calorimetry (DSC), and samples with volume 1 cm^3 for the mass density measurements. Furthermore, rectangular samples with dimensions 10 mm × 2 mm × 0.13 mm were cut for the electric conductivity measurements. EDX of the breaking edge of one of these samples showed a grain size in the range of 110 μm. The disc samples were polished with emery paper to remove the thin brass layer residual from the WEDM process. Rolled U8Mo foils were produced by slicing samples from the cast ingot; the slabs were rolled down from about 2.5 mm to 0.6 mm in a preliminary process at around 1000 °C to achieve dynamic recrystallization and restore the U8Mo metallurgical structure. Subsequently, the slabs were thinned to 250 μm by cold rolling. The produced foils show the U8Mo γ-phase and grain sizes in the range of 25 μm [7]. These foils were cut to slabs of 2 mm width and 12 mm length and polished by a grinding disc with emery paper and subsequently with 3 μm and 1 μm diamond emulsion to receive sample thicknesses in the range of 200 μm.

3. Sample characterization

The samples' chemical composition was determined by ICP-AES at the Institut für Radiochemie (Garching, Germany), showing a Mo content of 8.08 ± 0.45 wt.% and U content of 91.9 ± 0.45 wt.%.

The crystal structure was analyzed by X-ray diffraction (XRD) by the Bragg–Brentano method. To account for diffraction pattern errors from surface unevenness, the samples were covered with a thin Si standard powder layer. While the UMo crystal structure for quenched U8Mo is not described in literature, a survey of the literature data showed the known crystal structures for alloys with similar Mo content to be either tetragonal primitive or bcc. Table 1 is an overview of the literature data; the Mo content of 8 wt.% in the examined samples corresponds to 20 at.% Mo.

Rietveld analysis [8] of the diffraction pattern based on the tetragonal P4/nbm lattice structure reported for 12 at.% Mo showed good accordance of the measured data, while the Ia – 3 structure published for 14 at.% Mo gave only partial accordance at $2\theta = 23.81°$. Thus, the XRD results suggest the crystal structure of the U8Mo γ-phase to be P4/nbm. The diffraction pattern fitted with both examined structures are shown in Fig. 1. The measured spectrum is given in red,[1] the calculated fitting curve in black, the difference between measured and calculated curve in blue and the Bragg positions of the respective structures in green.

The fitting parameters used for the diffraction pattern analysis as well as the lattice parameters are given in Table 2.

From the presented data, U8Mo is concluded to be P4/nbm tetragonal primitive with lattice constants a = 6.856 Å and c = 3.452 Å.

4. Experiment

4.1. Heavy ion irradiation

The range of ^{127}I with 80 MeV in U8Mo has been simulated with the TRIM transport code [9]. With the main energy loss of heavy ions by ionization for high ion energies and by target atom collisions for lower energies, the primary collision events in the U8Mo samples follow an inhomogeneous distribution which peaks at about 5 μm depth. To simulate the homogeneously spread radiation damage by nuclear fission, the ion damage region is required to be as wide and homogeneously as possible. That can be achieved by either variing the ions' kinetic energy, thus spreading their range, or by changing the ions' incident angles to receive a damage region that has a smaller distance to the sample's surface, measured parallel to the surface normal. Fig. 2 shows the iodine ions' final positions in the target for only one energy and incident angle

[1] For interpretation of color in Figs. 1 and 2, the reader is referred to the web version of this article.

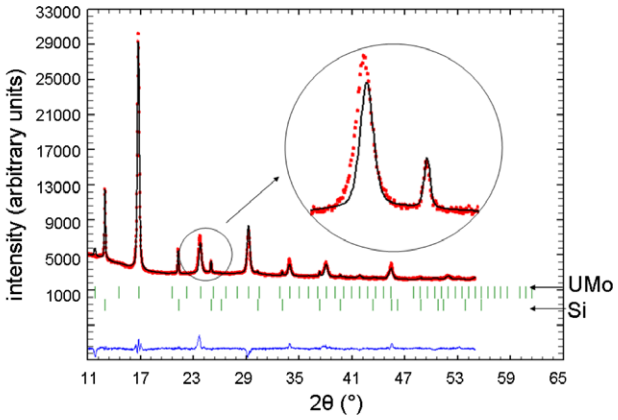

(a) XRD pattern fit based on cubic Ia-3 lattice structure

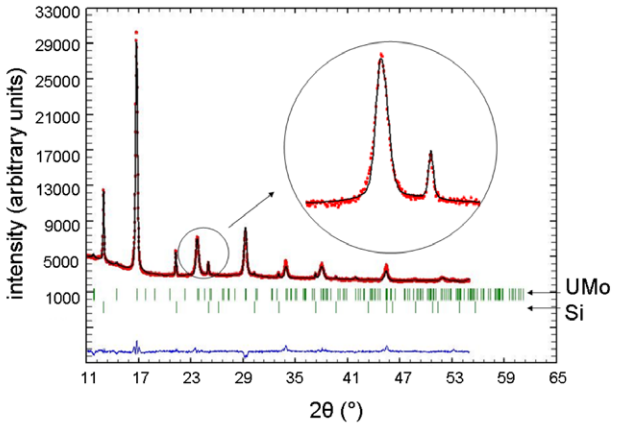

(b) XRD pattern fit based on tetragonal P4/nbm lattice structure

Fig. 1. XRD pattern fit based on different lattice structures.

Table 2
XRD fitting parameters.

Fitted structure	R_{Bragg}	χ^2	a (Å)	c (Å)
P4/nbm	0.101	3.63	6.8563(4)	3.4524(2)
Ia-3	0.138	6.13	6.8808(4)	

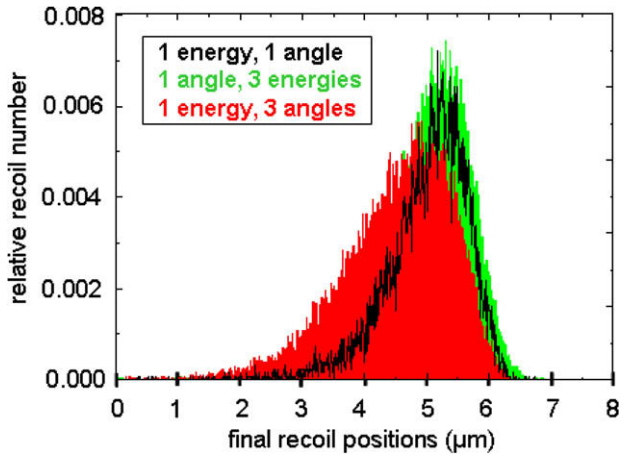

Fig. 2. Final iodine ion positions for different irradiation parameters.

0° in black, the distribution for incident angle 0° with the ion energies 70, 80 and 90 MeV in green and for 80 MeV with different incident angles 0°, 20° and 40° in red. It can be seen that the incident angle variation leads to a considerable broadening of the damage peak.

The irradiated samples were kept as thin as possible to maximize the measureable material changes caused by the thin damage region; samples with thicknesses between 130 μm and 200 μm were used.

The incident angle variation was provided by a turnable sample holder with defined angles to the beam. The sample heating by the ion beam current of about 200 nA was counteracted by a water cooling system in the sample holder. Test irradiation of a Pt100 thermal sensor with the same thermal connection to sample holder as the samples showed an average temperature of 85 °C which leads, with the sample holder's temperature being 20 °C, to an assumed surface temperature during irradiation of about 150 °C. The pressure during irradiation was in the range of 1×10^{-6} mbar.

The fission product density of the FRM II fuel at the targeted nuclear burnup is 2.3×10^{21} fission products per cm^3 in the fuel meat. Correlated to the small damage peak volume in the sample, that corresponds to an ion fluence of 9×10^{17} cm^{-2}.

4.2. Thermal conductivity measurements

To calculate the thermal conductivity of unirradiated U8Mo, its mass density, specific heat capacity and thermal diffusivity were measured.

The specific heat capacity c_p was determined by a power compensation differential scanning calorimetry ("DSC") setup at AREVA NP in a temperature range from 100 °C to 400 °C. The sample was kept under argon gas and was heated with a rate of 10 K/min, with one measurement value taken per second.

U8Mo's mass density ρ was determined by weighting an U8Mo sample with a volume of about 1 cm^3 under air and water, respectively, and calculating its mass density from the measured mass difference. The used measurement setup was provided by AREVA NP.

For the determination of the thermal diffusivity κ, a laser flash setup of AREVA NP was used. Two U8Mo discs with diameter 8.39 mm and thicknesses of 0.7 mm and 2.0 mm, respectively, were examined to exclude a measurement influence of the samples' thickness. To measure the thermal diffusivity in dependence of the temperature, the samples were heated to 240 °C and the measurements were done during the cooling process. Thus, thermal diffusivity data were received in a temperature range from 50 °C to 230 °C.

From the measured values, the thermal conductivity was received by Eq. (1).

$$\lambda = \kappa \cdot \rho \cdot c_p \tag{1}$$

Heat conduction in metals is given by electron and phonon heat transfer. Thus, an alternative to experimentally determine a metal's thermal conductivity is to measure the sample's electric conductivity σ and to calculate the electron based part of the thermal conductivity, λ_e, by the Wiedemann-Frantz law (see Eq. (2)), in dependence of the sample's temperature T.

$$\lambda_e = \frac{\pi^2 k_B^2}{3e^2} T\sigma \tag{2}$$

This method was used for the irradiated U8Mo samples with thicknesses in the range of 200 μm that were too thin for laser flash measurements.

The electric conductivity of U8Mo was determined by a four-wire method. Two alumel–chromel thermocouples were spot-

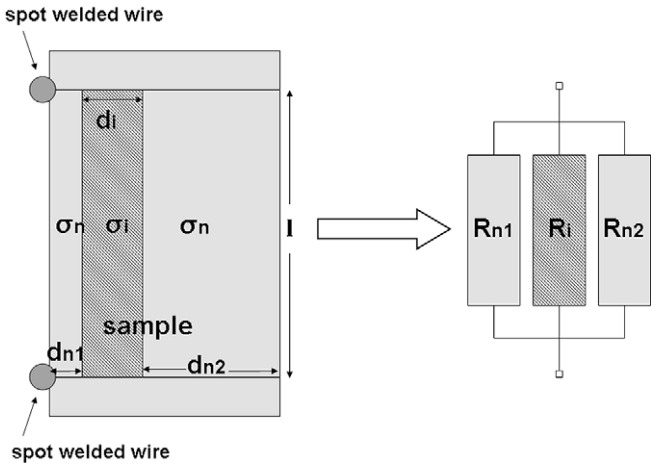

Fig. 3. Parallel resistance model for irradiated samples.

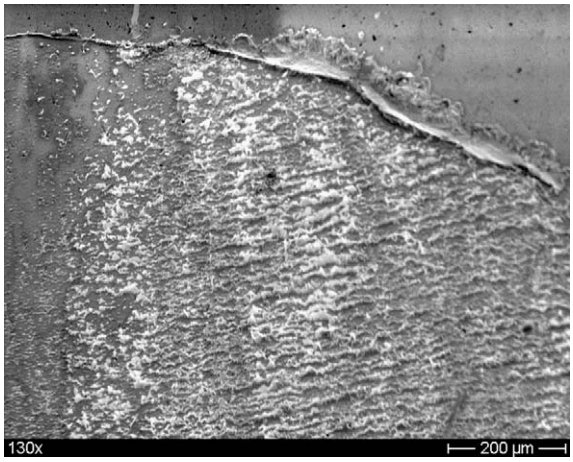

Fig. 4. Surface ripples after angular irradiation.

welded on rectangular U8Mo samples with dimensions 2 mm × 12 mm and thicknesses between 130 µm and 200 µm. For a given alternate current I with frequency 170 Hz and known sample dimensions, the electric conductivity of the samples can be calculated from the measured voltage drop between the wire pairs. The setup was kept at room temperature at 10^{-2} mbar to avoid temperature fluctuations by convection.

The resistivity of the damage region in the irradiated samples can be calculated by assuming the sample to be a parallel resistance of two non-irradiated layers and one irradiated layer in between, as described by Fig. 3.

Thus, the electric conductivity of the irradiated layer shown shaded, σ_i, can be calculated from the measured electric conductivity of the whole sample, σ_{tot}, the thicknesses of the different material layers d_j and the measured electric conductivity of the non-irradiated material, σ_n, as given in Eq. (3).

$$\sigma_i = \frac{d_{tot}}{d_i}\sigma_{tot} - \frac{d_{n1}+d_{n2}}{d_i}\sigma_n \tag{3}$$

5. Results and discussion

5.1. Post irradiation examination

For the samples irradiated under an incident angle differing from 0°, a rippled surface structure was observed that has also been reported by Wieschalla et al. [5] and Hou and Klaumünzer [16] (see Fig. 4); for the U8Mo samples irradiated at incident angle 0°, ion beam hammering led to a smoothing of the sample's surface.

Since a change in the surface geometry can influence the electric conductivity measurements, the irradiation was started at the highest incident angles and stopped at 0°; thus, the ion beam hammering smoothed the surface again.

X-ray diffraction was done with two irradiated rolled samples to examine possible changes during irradiation; the diffraction pattern were fitted based on the P4/nbm lattice structure observed for non-irradiated U8Mo (see Fig. 5).

With the attenuation coefficients of uranium and molybdenum for the Mo K_α-line being $\mu_U = 1808\ cm^{-1}$ and $\mu_{Mo} = 188\ cm^{-1}$, the U8Mo attenuation coefficient is given by the mean weighted with the atomic content: $\mu_{U8Mo} = 1485\ cm^{-1}$. That corresponds to a mean X-ray range from 0.3 µm to 1.7 µm for the examined X-ray incident angle range of 3–30°. With the signal being damped by a factor 1/e at the mean range, signals from deeper layers in the material, as the damage region around 5 µm, can still be expected.

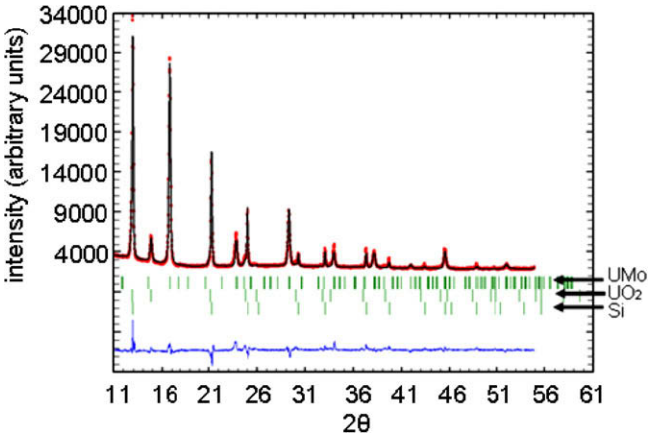

Fig. 5. XRD pattern of irradiated U8Mo, fit based on P4/nbm lattice structure.

As compared to the unirradiated samples, an additional phase, face-centered cubic UO_2, was found on the samples' surface.

Table 3 gives the fitting parameters, the measured lattice parameters and the ion fluence on the irradiated samples.

The diffraction pattern of the irradiated samples is in good accordance with the P4/nbm lattice structure. Thus, it can be concluded that a phase change does not occur during irradiation. However, a change of both a and c lattice parameters is observed for the irradiated samples. The unit cell volume decrease by irradiation is 0.34% for sample 1 and 0.41% for sample 2. Also, the ratio of the lattice parameters increases, by 1.1% for sample 1 and 0.30% for sample 2.

Table 3
XRD fitting parameters: irradiated and unirradiated rolled U8Mo.

Sample	Unirradiated	Irradiated 1	Irradiated 2
Fluence (cm^{-2})	0	9.0×10^{17}	9.9×10^{17}
R_{Bragg}	0.101	0.098	0.098
χ^2	3.63	4.13	8.00
a (Å)	6.8563(4)	6.8747(5)	6.8552(5)
c (Å)	3.4524(2)	3.4235(4)	3.4409(4)
a/c	1.986	2.008	1.992
Volume, a^2c (Å^3)	162.36(2)	161.80(3)	161.70(3)

5.2. Thermal conductivity

The thermal diffusivity of unirradiated U8Mo was measured by the laser flash method in the temperature range between 50 °C and 230 °C for two samples with different thickness. Data was taken at intervals of about 25 °C with about 10 measured values for each temperature region. The measurement values are given in Fig. 6 and show a linear increase with the temperature in the analyzed temperature range.

The temperature dependence can be fitted with a curve following Eq. (4), with the temperature given in °C.

$$\kappa = (4.08 \pm 0.14)\ \frac{\mathrm{mm}^2}{\mathrm{s}} + (0.0175 \pm 9.7 \times 10^{-5})\ \frac{\mathrm{mm}^2}{\mathrm{s}\,^\circ\mathrm{C}} \cdot T \qquad (4)$$

The specific heat capacity of an U8Mo sample with mass 781 mg was determined with the DSC setup; the data have been taken in the temperature range between 100 °C and 400 °C and at a heating rate of 1 K/min. Fig. 7 shows the received data.

In the examined temperature range, the data can be described by a constant value of 0.155 J/gK within the measuring accuracy.

The mass density of an unirradiated U8Mo sample with mass 9.7 g was measured several times at ambient temperature and has a value of $\rho_{\mathrm{U8Mo}} = (17.282 \pm 0.0497)\ \frac{\mathrm{g}}{\mathrm{cm}^3}$. For temperatures above ambient temperature, the density decreases by thermal expansion. As the thermal volume expansion coefficient for U8Mo is not available in the literature, it is approximated by the instantaneous coefficients of longitudinal and transversal linear expansion for U10Mo [27]. The volume expansion coefficient is calculated from these literature values by $\alpha_V = \alpha_L + 2\alpha_T$; the temperature dependence for 50–300 °C is given by the regression line in Eq. (5).

$$\alpha_V = [(34.25 \pm 0.089) + (0.040 \pm 3.6\mathrm{E}-4) \cdot T] \times 10^{-6}\ \mathrm{K}^{-1} \qquad (5)$$

The thermal conductivity of unirradiated U8Mo is calculated according to Eq. (1), with the mass density's temperature dependence calculated using the thermal volume expansion coefficients according to Eq. (5); as the thermal diffusivity data show the highest temperature dependence, the thermal conductivity values have been calculated for the temperature intervals given by the diffusivity measurements. At temperatures where two diffusivity values were received by the different samples, they were averaged. The received values are shown in Fig. 8.

The thermal conductivity shows a linear increase with the temperature in the examined temperature range that can be described by a curve following Eq. (6).

$$\lambda = (12.17 \pm 0.26)\ \frac{\mathrm{W}}{\mathrm{mK}} + (0.038 \pm 0.0021)\ \frac{\mathrm{W}}{\mathrm{mK}\,^\circ\mathrm{C}} \cdot T \qquad (6)$$

The temperature is given in °C.

Fig. 9 gives an overview of the known thermal conductivity values for UMo alloys with a molybdenum content close to 8 wt.%.

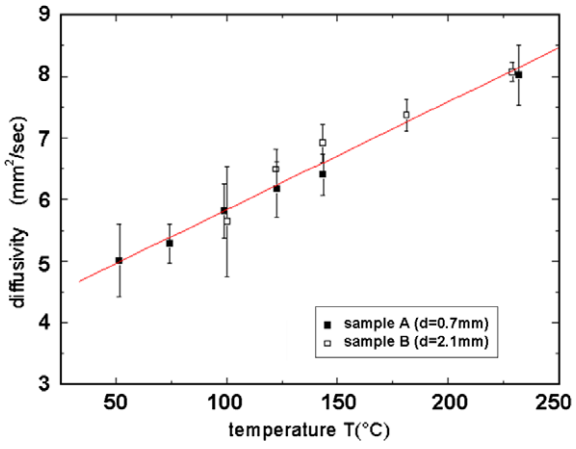

Fig. 6. Thermal diffusivity of unirradiated U8Mo.

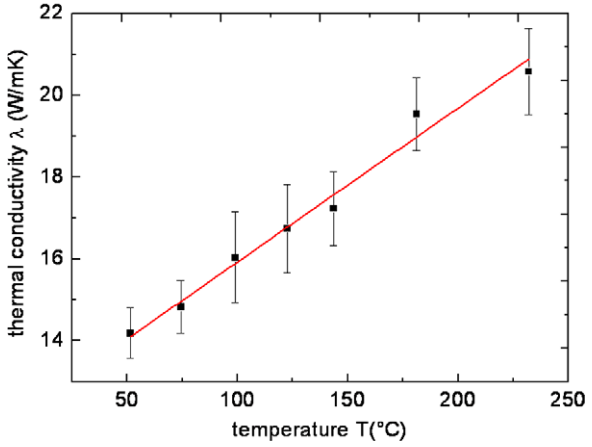

Fig. 8. Thermal conductivity of unirradiated U8Mo.

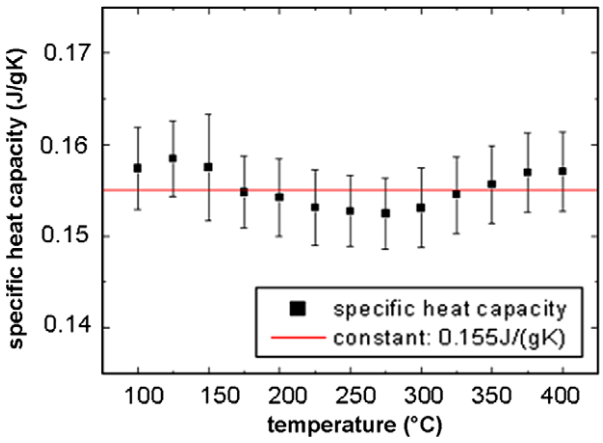

Fig. 7. Specific heat capacity of non-irradiated U8Mo.

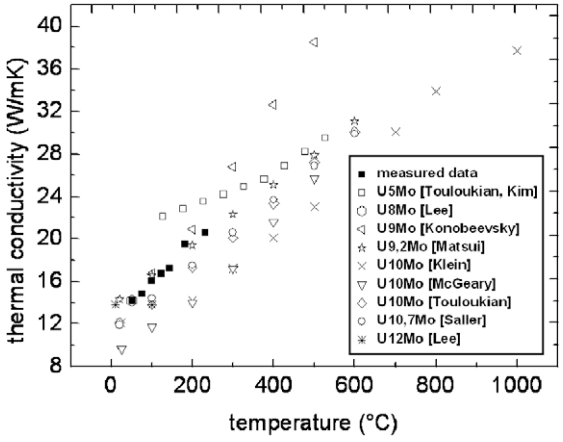

Fig. 9. Thermal conductivity of unirradiated U8Mo: comparison with literature data; measurement errors are given in Fig. 8.

While the thermal conductivity for UMo alloys with 5 wt.% Mo [17,18] is higher than for U8Mo between 50 °C and 230 °C, the alloys with 10 or more wt.% Mo [18–21] have a lower thermal conductivity. The literature values for 9 wt.% [22] and 9.2 wt.% [23] show good agreement with the measured U8Mo data. For 8 wt.% Mo, only a single value can be found as 14.2 W/mK for 0–100 °C [24]. That value is in good accordance with the measured data at 50 °C.

Recently presented data [25] for 7 wt.%, 10 wt.% and 12 wt.% Mo are in good accordance with the measured values.

The electric conductivity of unirradiated U8Mo was examined for one cast sample and four rolled samples; two of the measured samples were irradiated with iodine and their electric conductivity measured again afterwards. From the TRIM simulation for the irradiation under different incident angles (see Fig. 2), it can be estimated that the damage peak region has a thickness of 4 μm with a distance of 2.5 μm of its outer rim to the sample's irradiated surface. The region of 4 μm contains the major part of the incident ions. Then, the electric conductivity of the heavily irradiated layer can be calculated by the parallel resistance model according to Eq. (3).

Literature data is not available for the electric conductivity of U8Mo; however, there is data for 10 wt.% Mo [26], with the alloy in the $(\alpha+\delta)$ phase and the γ-phase, respectively. These values are given with the measured data for unirradiated U8Mo in Fig. 10.

The measured values for the electric conductivity show good accordance from sample to sample; in particular, the electric conductivity of the cast sample "'B2" is consistent with the rolled samples "F2" to "F5". Thus, it can be concluded that microstructural differences between the cast and the rolled samples, e.g. different grain geometries, grain sizes, homogeneity or textures, do not significantly influence the electric conductivity measurements. However, the measured value for sample "F2" deviates from the other samples. A possible explanation is a local variation of the sample's microstructure from the other samples that could have been inserted by unintended cold work through sample bending during preparation or by untypically low binding between sample and spot welded wires due to deviating spot welding parameters. As compared to the data for 10 wt.%, the measured electric conductivity for U8Mo is lower. A lower value can be expected, as Fig. 9 shows a lower total thermal conductivity for higher Mo contents. However, differing material treatment and defect concentrations cannot be excluded as a factor influencing that difference because sample preparation details are not provided in the literature for the U10Mo data [26].

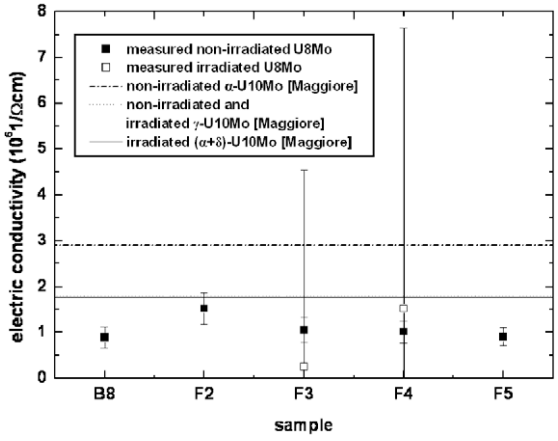

Fig. 10. Electric conductivity of cast ("B") and rolled ("F") U8Mo samples.

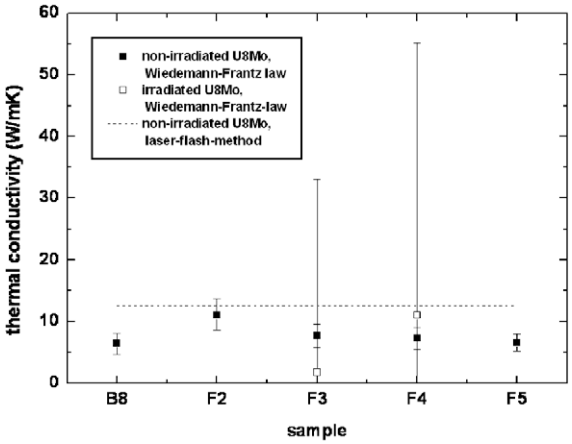

Fig. 11. Thermal conductivity of unirradiated and irradiated cast ("B") and rolled ("F") U8Mo samples.

The received values for the electric conductivity of unirradiated and irradiated U8Mo are then used to calculate the electronic part of the thermal conductivity by the Wiedemann-Frantz law (see Eq. (2)). The corresponding values for the five samples are shown in Fig. 11; as a comparison, the thermal conductivity extrapolated from the laser flash data to the ambient temperature of about 23 °C is shown in the plot, too. With the laser flash data in good accordance to the literature values, that can be used as a reliable reference.

As compared to the total thermal conductivity measured by laser flash, the values calculated by the Wiedemann-Frantz law are lower which is to be expected because the purely phonon based part of the thermal conductivity is not taken into account. The values calculated by the parallel resistance model show very large errors that are due to the low thickness of the irradiated layer that is very thin as compared to the whole sample. It has to be concluded that for samples of the used dimensions, changes of the electron based part of the thermal conductivity cannot be resolved. A solution to that problem can be expected by the use of thinner samples with thicknesses in the range of the damage peak region of the heavy ions, which could be produced by sputtering. Due to mechanical instabilities, these samples should be brought upon an electrically insulating substrate.

While the effect of irradiation on the thermal conductivity of γ-U8Mo is not reported in literature, some measurements exist for γ-U10Mo. Fackelmann et. al describe a decrease of U10Mo's thermal conductivity from 17 W/mK for unirradiated material to 15 W/mK for material with burn-up between 0.36 and 1.2 at.% [27]. Assuming that the thermal conductivity of U8Mo shows the same trend, the irradiated layer of sample F3 shows a more dependable value of the thermal conductivity than sample F4.

6. Conclusion

The objective of this work was the characterization of different physical properties of U8 wt.%–Mo with regard to its possible application as nuclear fuel for high flux reactors.

The crystal structure of rolled U8Mo was determined to be P4/nbm tetragonal with lattice parameters $a = 6.8563(4)$ Å and $c = 3.4524(2)$ Å. Irradiation with 80 MeV ^{127}I to fluences in the range of 9×10^{17} cm^{-2} led to a change of the lattice parameters, causing a decrease in unit cell volume. Also, fcc UO_2 was found on the samples after the ion irradiation.

The thermal diffusivity of U8Mo was determined by the laser flash method in the temperature range of 50–230 °C to follow

the linear Eq. (4). The specific heat capacity in the temperature range of 100–400 °C has a constant value of 0.155 J/g K within the measuring accuracy. Cast U8Mo showed a mass density of $(17.282 \pm 0.0497)\ g/cm^3$ at room temperature. From these values, the thermal conductivity of U8Mo has been calculated to follow the linear Eq. (6) in the temperature range of 5–230 °C. The data show excellent agreement with the literature data for UMo alloys with similar Mo content.

By a four-wire method, the electric conductivity of U8Mo has been measured at room temperature; then, the electron based part of the thermal conductivity has been calculated by the Wiedemann-Frantz law to be in the range of $1 \times 10^6\ (\Omega K)^{-1}$. The thus received values for the thermal conductivity are in the range of 7 W/m K, depending on temperature. The electron based part of the thermal conductivity of two rolled irradiated U8Mo samples was measured the same way. Due to the very thin damage peak region in the samples, the measurement errors are large. Thus, changes of the thermal properties of U8Mo by irradiation cannot be resolved by that method. However, successful experiments can be expected by the described method for samples with thicknesses in the range of 20 μm.

Acknowledgements

This work has been supported by common funds of the German BMBF. Prof. S.S. Schmahl (LMU, Munich, Germany) provided the X-ray diffraction setup. Dr. C. Lierse and F. Klein (Institut für Radiochemie, Garching, Germany) offered the chemical analysis and the EDX measurements.

References

[1] Reduced Enrichment for Research and Test Reactors (RERTR), May 2009 <http://www.rertr.anl.gov>.
[2] W. Petry, A. Röhrmoser, J.L. Falgoux, C. Jarousse, P. Boulcourt, A. Chabre, S. Dubois, P. Lemoine, S. Van den Berghe, A. Leenaers, IRIS-TUM Program on Full Size Plates-UMo Dispers, RRFM, 2008. <www.rrfm2008.org>.
[3] A. Röhrmoser, W. Petry: Reduced Enrichment Program for FRM II, Actual Status and a Principal Study of Monolithic Fuel for FRM II; RRFM, 2006. <www.rrfm2006.org>.
[4] E. Welcomme, H. Palancher, P. Martin, J. Allenou, F. Charollais, M.C. Anselmet, C. Valot, P. Lemoine, R. Tucoulou, C. Jarousse, L. Beck, R. Jungwirth, W. Petry, Heavy Ion Irradiation of UMo7/Al Fuel: Methodological Approach, RRFM, 2009. <www.rrfm2009.org>.
[5] N. Wieschalla, A. Bergmaier, P. Böni, K. Böning, G. Dollinger, R. Grossmann, W. Petry, A. Röhrmoser, J. Schneider, J. Nucl. Mater. 357 (2006).
[6] R. Jungwirth, W. Petry, W. Schmid, L. Beck, A. Bergmaier, Progress in Heavy-ion Bombardement of U–Mo/Al Dispersion Fuel, RRFM, 2008. <www.rrfm2008.org>.
[7] C. Jarousse, P. Lemoine, W. Petry, A. Röhrmoser, Monolithic UMo full size prototype plates manufacturing development, RERTR, 2005. <http://www.rertr.anl.gov/RERTR27/index.html>.
[8] H.M. Rietveld, J. Appl. Crystallogr. 2 (1969) 65–71.
[9] J.F. Ziegler, November 2008. <www.srim.org>.
[10] N. Vigier, C. Den Auwer, C. Fillauy, A. Maslennikov, H. Noel, J. Roques, D.K. Shuh, E. Simoni, T. Tyliszczak, P. Moisy, Chem. Mater. 20 (2008) 3199–3204.
[11] H.L. Yakel, A review of X-ray diffraction studies in uranium alloys, in: Proceedings of the Third Army Materials Technology Conference, 1974.
[12] D. Stewart, G.I. Williams, J. Nucl. Mater. 20 (1966) 262–268.
[13] K. Tangri, Mem. Sci. de la Rev. Metall. 58 (1961) 469–477.
[14] E.K. Halteman, Acta Crystallogr. 10 (1957) 166–169.
[15] C. Bernuy-Lopez, M. Allix, C.A. Bridges, J.B. Claridge, J.M. Rosseinsky, Chem. Mater. 19 (2007) 1035–1043.
[16] M.D. Hou, S. Klaumünzer, Nucl. Instrum. Meth. Phys. Res. B 209 (2003) 149–153.
[17] E.L. Francis, Uranium Data Manual, UKAEA Report IGR-R/R-287, 1958.
[18] Y.S. Touloukian, R.W. Powell, C.Y. Ho, P.G. Klemens, Thermophysical Properties of Matter, IFI/Plenum, 1971.
[19] J.L. Klein, in: A.R. Kaufmann (Ed.), Nuclear Reactor Fuel Elements, 1962.
[20] R.K. McGeary, Development and Properties of Uranium-base Alloys Resistant to Corrosion in High-temperature Water, USAEC Report WAPD-127 Part I, 1955.
[21] A. Saller, R.F. Dickerson, A.A. Bauer, N.E. Daniel, Properties of a Fissium-type Alloy, Battelle Memorial Institute, Report BMI-1123, 1956.
[22] S.T. Konobeevsky, Some physical properties of uranium, plutonium, and their alloys, in: Proceedings of the Second UN International Conference on the Peaceful Uses of Atomic Energy, 1958.
[23] T. Matsui, T. Natsume, K. Naito, J. Nucl. Mater. 167 (152) (1989).
[24] S.-H. Lee, J.-C. Kim, J.-M. Park, H.-J. Ryu, C.-K. Kim, An Investigation of the Thermophysical Properties of U–Mo Dispersion Fuel Meats, RERTR, 2000. <www.rertr.anl.gov>.
[25] D.E. Burkes, D.M. Wachs, D.D. Keiser, J.-F. Jue, M.A. Okuniewski, F.J. Rice, R. Prabhakaran, Update on Fresh Fuel Characterization of U–Mo Alloys, RRFM, 2009. <www.rrfm2009.org>.
[26] S.G. Maggiore, Radiation damage in reactor materials, in: Proceedings of the Symposium on Radiation Damage in Solids and Reactor Materials, IAEA, 1962.
[27] J.M. Fackelmann, A.A. Bauer, D.P. Moak, Literature Survey on Dilute Uranium Alloys for Sandia Booster Concept to Sandia Corporation, 1969.